

Activation Quantization of Vision Encoders Needs Prefixing Registers

Seunghyeon Kim¹, Jinho Kim², Taesun Yeom¹, Wonpyo Park³, Kyuyeun Kim³, Jaeho Lee^{1*}
 POSTECH¹, Dankook University², Google³

{shkim0418, tsyeom, jaeho.lee}@postech.ac.kr, sunder990@dankook.ac.kr
 {wppark, kyuyeunk}@google.com

Abstract

Transformer-based vision encoders—such as CLIP—are central to multimodal intelligence, powering applications from autonomous web agents to robotic control. Since these applications often demand real-time processing of massive visual data, reducing the inference cost of vision encoders is critical. Quantization offers a practical path, but remains challenging even at 8-bit precision due to massive-scale activations (i.e., outliers). In this work, we propose RegCache, a training-free algorithm that mitigates outliers in large-scale pretrained vision encoders and serves as a plug-in module that can be applied on top of other quantization methods. The proposed RegCache introduces outlier-prone yet semantically meaningless prefix tokens to the target vision encoder, which prevents other tokens from having outliers. Notably, we observe that outliers in vision encoders behave differently from those in language models, motivating two technical innovations: middle-layer prefixing and token deletion. Experiments show that our method consistently improves the accuracy of quantized models across both text-supervised and self-supervised vision encoders.

1. Introduction

Transformer-based vision encoders, such as CLIP or DINOv2, lie at the core of modern multimodal intelligences [27, 29]. Leveraging the scalability of vision transformer (ViT) backbone [10], these models can be pretrained with massive amount of data and computation, yielding highly informative and versatile visual features. Today, those vision encoders are now being adopted as plug-and-play components across diverse multimodal applications, ranging from autonomous web agents to robotic control [28].

Lowering the inference cost of vision encoders is essential, as their applications often require real-time processing of visual signals on edge devices, e.g., on-device robotic control [16]. Post-training quantization (PTQ) is a

promising solution for this purpose, as the technique can substantially reduce the memory and computation burden of the models without any additional training [6]. In particular, the activation quantization of vision encoders is of significant importance; the models are typically non-autoregressive and run on edge hardwares, and thus more likely to be in compute-bound scenarios than in memory-bound one.¹ Quantizing both activations and weights enables the replacement of high-precision matrix multiplications with low-precision operations (e.g., int8), effectively reducing the required computation and energy.

However, quantizing the activations of vision encoders is challenging due to the *outlier* activations, i.e., few activations with extremely large magnitude. In particular, large-scale vision encoders tend to have outliers emerging in a small number of channels at the middle-to-final blocks of the models [32]. These outliers force the quantization range of the activations to be much larger than usual, leading to a significant quantization error. Strategies for outlier-robust quantization have been actively studied, particularly in the context of large language models (LLMs), which also suffers from outliers similarly [9, 20, 37]. These approaches, however, typically involve applying different precision or quantization range to different tokens or channels. Such operations incur significant overhead and are difficult to be applied for static activation quantization. [4, 31].

An emerging alternative approach is to directly mitigate outliers in the model by prefixing *attention sink* tokens, i.e., semantically meaningless tokens—such as $\langle \text{BOS} \rangle$ or $\langle \text{SEP} \rangle$ —which collect large attention from other tokens [32, 38]. Recent studies on LLM quantization observe that adding the activations of these sink tokens as a prefix in each attention layer can dramatically reduce the activation magnitudes of other tokens, thereby boosting the post-quantization accuracy of large language models [4, 31, 40].

Naturally, one may ask: Can we mitigate the outliers in vision encoders by prefixing attention sinks? Unfortunately,

¹This is in contrast with the scenarios of autoregressive large language models running on GPU servers. The inference is memory-bound and the weight-only quantization becomes effective.

*Corresponding Author.

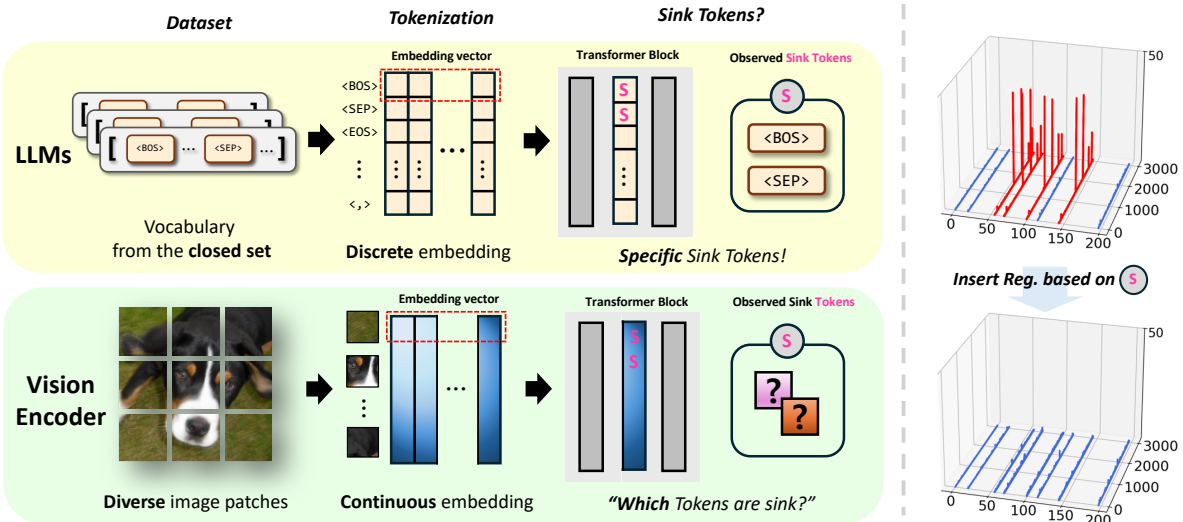


Figure 1. **(Left) Sink tokens in LLMs vs. vision encoders.** In LLMs, well-known sink tokens exist in a closed-set vocabulary. In contrast, vision encoders take image inputs composed of diverse patches that are continuously mapped into an embedding space, making the discovery of sink tokens more challenging. **(Right) Activation magnitudes at the input of the 8th layer of CLIP-B/16, with and without RegCache (ImageNet-1k).** RegCache discovers and inserts register token to quantization-sensitive layers, not as an input. This operation mitigates outliers, thereby narrowing the dynamic range and enabling more effective activation quantization under low bitwidths.

it remains unclear which vision encoder token (i.e., patch embedding) can play an analogous role to attention sinks in language models. Unlike language models, most existing vision encoders are not pretrained with tokens that are designated to be semantically meaningless. A recent line of works report that adding such meaningless tokens—called “registers”—during the training provide meaningful advantages in term of the interpretability of vision transformers [7]. However, it is still a rare practice to include such registers for vision encoders (Fig. 1, left).²

Contribution. In this work, we introduce **RegCache** (Register Caching), a novel prefix-based outlier mitigation algorithm for quantizing pretrained vision encoders. RegCache is inspired by the following empirical observation about the emergence of registers in vision encoders:

Sink tokens emerge gradually from the **middle** layers of vision encoders, giving rise to outliers. Moreover, such tokens are **highly similar across images**, and thus can be used as a **universal middle-layer register** for any input image at test phase.

Based on this observation, RegCache mitigates outliers by discovering and prefixing these middle-layer registers to the target vision encoder, in the form of a pre-computed key-value cache. Importantly, unlike in LLM prefixing [31], the tokens are prefixed only for middle-to-final layers, and do

²In this regard, DINOv3 is a pleasant exception [30].

not affect the early layers. Furthermore, RegCache additionally deletes out the tokens that have gradually became attention sink, which are likely to suffer from outliers in subsequent blocks. By such adding-and-deleting of tokens, RegCache replaces internally emerging sink tokens with external pre-computed caches, so that sink tokens do not affect the activation quantization range of the model. The whole procedure does not require any further training of the vision encoder, rendering RegCache a versatile and go-to method.

Throughout our experiments, we apply RegCache to diverse text- and self-supervised vision encoders and pair it with recent PTQ methods for ViTs, which alone suffer from performance degradation caused by large activation outliers. We observe that combining RegCache with recent PTQ methods consistently improves the prediction accuracy of the quantized vision encoder across all considered setups.

2. Related work

Outlier in large-scale transformers. In large-scale transformers, it has been observed that some activation magnitudes at certain layers become significantly larger than others; this phenomenon is referred to as the emergence of outliers [2, 9, 17, 33]. Sun et al. [32] conducts a systematic study of outliers, to show that they arise due to the softmax in the self-attention mechanism in LLMs and ViTs. They show that certain tokens in LLMs, e.g., <BOS> or <SEP>, consistently exhibit extreme activation magnitudes. Several works in the vision domain show that outlier to-

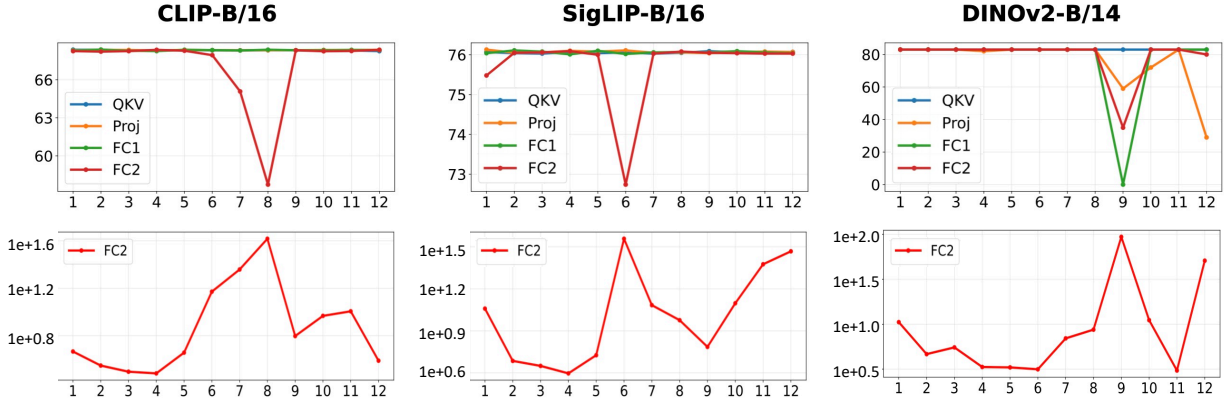


Figure 2. **(Top) Layerwise quantization sensitivity (%)**. We plot the zero-shot ImageNet-1k accuracy of various vision encoders when we quantize only one layer to W8A8. **(Bottom) Maximum norm of the FC2 layer input tokens for each layer**. We plot the largest ℓ_∞ -norm of all tokens in an image in a logarithmic scale, averaged over the ImageNet-1k validation set. The layer which is sensitive to quantization coincides with where activation outliers appear. For both plots, the x-axis denotes the index of the transformer block.

tokens in ViTs typically correspond to uninformative uniform background patches, and that removing them can improve internal representations [7, 14, 25]. In contrast to LLMs, it remains unclear which “specific” visual tokens give rise to outliers in ViT-based vision encoders, given different characteristics between language and image data (e.g., different images have different backgrounds). In this work, we find that, across a wide range of vision encoders, outlier tokens typically emerge in intermediate blocks and exhibit similar features across images, enabling them to be pre-computed for a given use-case, such as PTQ.

Improving vision transformers via controlling attention sink tokens. Attention sinks, first highlighted by Xiao et al. [38], are tokens with little or no semantic information that nevertheless attract excessive attention in both LLMs [13] and ViTs [7]. In ViTs, critically, these sink tokens act as noise in the attention map, hindering the model’s ability to capture relations between different patches and thereby degrading downstream visual performance [7, 14, 15, 25]. Seminal work by Dariset et al. [7] adds register tokens that disperse abnormally high attention scores concentrated on sink tokens and thus mitigate attention sinks during training. More recently, Jiang et al. [14] suggest identifying register neurons (i.e., specific channels in the linear layers of ViT blocks) before training and “delete-and-paste” the maximum value of register neurons to zero-initialized token at test time. Taking a slightly different perspective, we ask how to leverage sink tokens which strongly correspond to activation outliers to improve activation quantization. From this perspective, our strategy can be viewed as using a (pre-computed) sink token from another image to absorb outliers in an actively processed image.

Post-training quantization for vision transformers. There have been a lot of effort to reduce the inference cost of large-scale ViT-based models via PTQ [35, 36, 41]. Early PTQ methods for ViTs address quantization errors by assigning dynamic bitwidths to self-attention-sensitive layers [23]. Subsequent studies identify that low PTQ performance of ViTs are due to outliers, originating from operations such as LayerNorm, softmax, and GELU activation. RepQ-ViT [19] and PTQ4ViT [42] propose novel quantization schemes to isolate and minimize the impact of outliers. Methods such as NoisyQuant [22] attempt to alleviate the tail-like behavior of activations by adding noise or reshaping distributions. FIMA-Q [35] introduces a novel round-function optimization for PTQ. Despite such efforts, these approaches are still highly sensitive to the magnitude of outliers. Our approach handles outliers via token prefixing and when integrated with existing methods, enables them to operate within a further reduced dynamic range, thereby lowering quantization error.

3. A closer look at outliers in vision encoders

Outliers in vision encoders emerge at seemingly random background patch tokens in given images, while in LLMs they tend to appear at specific location or types of tokens [7, 32]. Such lack of specificity makes it difficult to mitigate the outliers in vision encoders through prefixing [31], as the strategy requires caching the tokens that induce outliers universally across any input that can be given to the model at the test time (i.e., registers). In this section, we provide two observations suggesting that an alternative strategy may be effective: “Find universal sink tokens in middle layers of the model, and prefix them in these middle layers.”

- Section 3.1: Layerwise quantization sensitivity in vision

encoders (i.e., the performance drop when quantizing individual layers of a transformer block) is particularly high in the middle layers where outliers emerge and low otherwise; thus, prefixing need not be applied in early layers.

- Section 3.2: We report an intriguing observation which sheds light on why such late emergence (i.e., middle layers) of outliers happen in vision encoders. Precisely, the observation suggest that: “vision encoders require early layers to process the image, in order to understand which tokens are semantically meaningless.”
- Section 3.3: In the middle layers where outliers begin to emerge, the pairwise cosine similarity of outlier tokens across different images becomes very high; thus, these tokens can act as universal registers.

3.1. Layerwise quantization sensitivity and outliers

We first analyze the quantization sensitivity of each layer in vision encoders, and establish connection to the emergence of outliers in activation (i.e., FC2 input). In Fig. 2 (top), we report the layerwise quantization sensitivity, measured as the zero-shot ImageNet-1k accuracy when the model is quantized to W8A8. We observe that quantization-sensitive layers—i.e., layers with substantial accuracy drop when quantized—are highly localized to the MLP projection layers in one or two middle layers. In DINOv2, the performance degradation is the sharpest, and takes place in other layers and blocks as well. Furthermore, as can be seen from Fig. 2 (bottom), these quantization-sensitive layers coincide with the layers where the activation outliers in the hidden states begin to emerge. Together, the plots suggest that outliers are indeed the driving factor of performance drops when quantizing vision encoders. In Sec. A, we further show the impact of outlier tokens under the quantization setup, highlighting the importance of mitigating such outliers for better quantization performance.

These findings extend and refine prior observations that vision encoders have high-norm tokens in the middle-to-later layers [7, 14]. In particular, we establish a concrete connection between the quantized accuracy and the high-norm behaviors. Furthermore, our findings suggest that FC2 activations or measuring quantization sensitivity directly may be useful in pinpoint the block where prefixing should be conducted. We provide the results on other vision encoders (OpenCLIP and SigLIP2) in Sec. E.

3.2. Why the middle layers?

A natural question arises here: Why do outliers in vision encoders emerge in the middle layers, while outliers in LLMs emerge in the early layers? We hypothesize that this is essentially due to the fact that it is not readily clear from the raw image tokens which are *semantically meaningless*—they become clearer after being processed by first several blocks of the vision encoder. This is in contrast with the

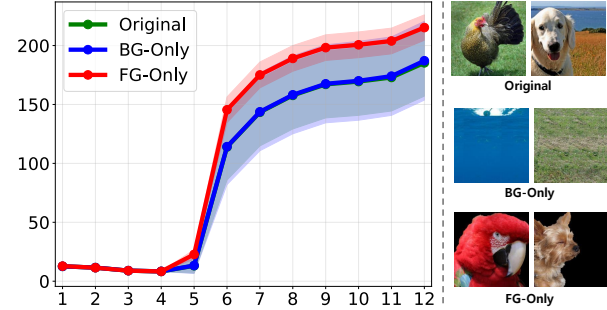


Figure 3. **Emergence of outliers in foreground- and background-only images on SigLIP-B/16.** Note that the curves for “original” and “BG-only” almost overlap.

case of LLMs, where some tokens are clearly meaningless even at the first glance, e.g., $\langle \text{BOS} \rangle$, $\langle \text{SEP} \rangle$ (see Fig. 1, left).

To validate this hypothesis, we design an experiment where we can compare the emergence of outliers for images where some patches are clearly meaningless, against those where the distinction is less clear. Precisely, using the test set of ImageNet-9 [39], we compare the outliers of the foreground-only images—where the background pixels are zero-ed out—to the vanilla images. In principle, in foreground-only images, the semantically meaningless patches should be identifiably more easily, i.e., with a smaller number of blocks for processing.

In Figure 3, we observe that the outliers in foreground-only images indeed emerge earlier and larger than in original case, supporting our hypothesis. In contrast, if we remove the foreground and keep the background only, the outlier behaviors did not change noticeably (i.e., they almost overlap). In Sec. J, we provide additional analysis of vision encoders trained with registers, in which the notion of the meaningless tokens is clear (and also predefined). In this case, we observe that these models behave similarly to LLMs, with outliers emerging from the early layers.

3.3. Universality of outlier tokens

Next, we take a closer look at the outlier tokens in the quantization-sensitive layer. Precisely, we measure the cosine similarity of the middle-layer FC2 input outlier tokens (i.e., having the largest ℓ_∞ -norm) collected for two images. We use 64 randomly sampled images from the ImageNet-1k validation split, and compute the mean pairwise cosine similarity.

From Tab. 1, we observe that outlier tokens are highly similar across different images, with the mean cosine similarity of 0.89. On the other hand, the normal tokens are much more dissimilar from each other, with only 0.26. This indicates that outliers share components that are largely independent of input image, and thus may represent universal

Table 1. Mean cosine similarity between tokens in SigLIP-B/16.

Token Type	Cosine sim.
Normal tokens	0.26 (± 0.10)
Outlier tokens	0.89 (± 0.07)

features that persist across samples. In Sec. B, we provide a theoretical explanation for this phenomenon, showing that it arises from (1) the large magnitude of the outliers and (2) the alignment of their locations (i.e., channels).

4. Method

Before describing our outlier mitigation method, recall two observations from the Sec. 3:

- Outliers in vision encoders tend to emerge in the middle layers (e.g., fully-connected layers in block 5–8), whereas for LLMs outliers emerge from the early layers.
- Sink tokens (i.e., outlier-prone) discovered in the middle layers tend to be similar across images.

Putting these together with prior observations in LLMs—prefixing additional sink tokens mitigate outliers in other tokens [31]—we arrive at the following hypothesis:

“Middle-layer sink tokens from another image can play a role similar to registers, and thus can help mitigating outliers in vision encoders.”

Based on this hypothesis, we propose RegCache (Register Caching), an outlier mitigation algorithm which replaces internally emerging sink tokens by inserting sink tokens discovered from reference images as registers. In a nutshell, RegCache operates in three steps (see Fig. 4).

- (1) **Curating** a set of register candidate tokens from a pool of reference images. ▷ Sec. 4.1
- (2) **Caching** the keys and values of selected register candidates to the sensitive layers. ▷ Sec. 4.2
- (3) **Deleting** internally emerging sink tokens to clean up remaining outliers. ▷ Sec. 4.3

RegCache does not involve any training or tuning of the model, and only conducts several rounds of validation on some reference task and data (will be discussed below). Thus, the algorithm does not require an excessive amount of training data or computational resource. At the inference phase, the algorithm adds and removes several tokens, which slightly affects the computational cost of the model. However, as we will see in Sec. H, this change is negligible, and the cost even decreases on average.

4.1. Curating

Given a pretrained vision encoder, we first identify the quantization-sensitive layer of the model. Then, we construct a curated set of register candidate tokens by selecting top- k tokens with largest sensitive-block activations, among all tokens taken from a pool of reference images.

Identifying the quantization-sensitive layer. As in Sec. 3.1, we quantize each layer of the given vision encoder separately, and select the one that leads to the lowest accuracy on some reference task as the quantization-sensitive layer. Here, if we have a specific base quantization algorithm (to be used after the outlier mitigation), we can use

the algorithm; otherwise, we will use the vanilla round-to-nearest quantization. The reference task is selected as one that is considered representative of visual understanding, e.g., classification on the ImageNet-1k training set.

Curating the set of register candidates. After identifying the quantization-sensitive layer, we construct the set of register candidate tokens, which are likely to play the role of a register when inserted to the quantization-sensitive layer. This is done by predicting on the a pool of reference images with the vision encoders and selecting tokens with the largest ℓ_∞ norm at the quantization-sensitive layer. More formally, let l_q denote the quantization-sensitive layer of the target vision encoder as identified through the sensitivity analysis described in Sec. 3.1, and let $\Phi_l(\mathbf{x})$ denote the set of tokens at the input of the l -th layer for an image \mathbf{x} . Then, we can construct the set of register candidates as follows.

$$\mathcal{S} = \text{argtopk} \left\{ \|\mathbf{z}\|_\infty \mid \mathbf{z} \in \Phi_{l_q}(\mathbf{x}), \text{ for some } \mathbf{x} \in \mathcal{I}_{\text{ref}} \right\}, \quad (1)$$

where \mathcal{I}_{ref} denotes the pool of reference images. In this paper, we use 50,000 images randomly drawn from the ImageNet-1k training split as this pool and set $k = 100$. As the sink tokens often emerge a few blocks before the quantization-sensitive layer, we also conduct a similar search for several blocks preceding the quantization-sensitive layer. We search up to three additional preceding blocks to construct register candidate sets for each block.

4.2. Caching

Having the set of register candidates \mathcal{S} constructed, we compose the register by simply averaging the key-value (KV) caches of the register candidate tokens $\mathbf{z}^* \in \mathcal{S}$. We then search for the optimal $\tau^* \in \mathbb{N}$, the number of times the register is copied and inserted into the target vision encoder. Precisely, the search is done as follows.

- First, we compute KV caches for each register candidate token $\mathbf{z} \in \mathcal{S}$, for blocks starting from the few layers before the quantization-sensitive block, as well as all subsequent blocks using the *unquantized* vision encoder.
- Then, we insert the averaged KV cache to the *quantized* vision encoder, with different number of copies. We vary τ within the range $\{1, 2, \dots, 15\}$ and select τ^* the one with the highest reference task accuracy.³ Here, as in Sec. 4.1, we consider classification on the training split of ImageNet-1k dataset as our reference task.

4.3. Deleting

Finally, we apply a *token deletion* process to the input of the quantization-sensitive block (i.e., the block where l_q is located) in the vision encoder. At the inference phase, this process removes the sink tokens that emerge among the image patch tokens, thus removing any remaining outliers.

³The total search cost of our algorithm is about 1 hour when using a naive RTN pseudo-quantization algorithm on an RTX 4090.

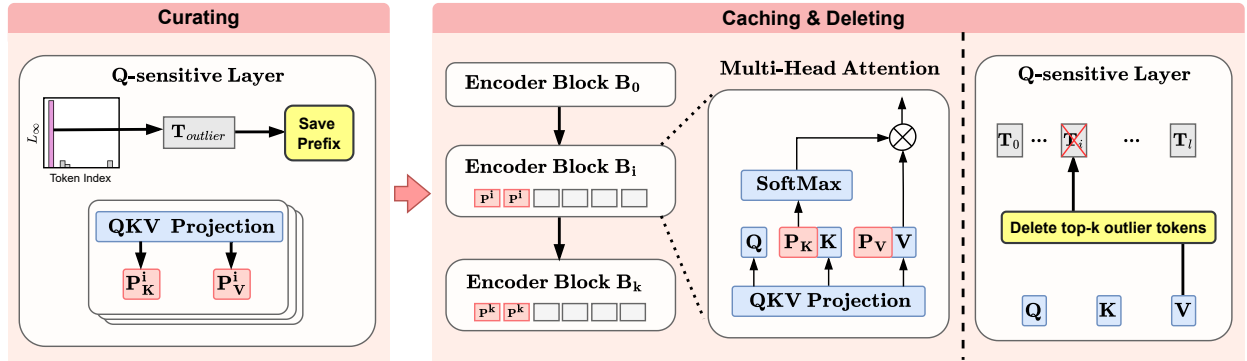


Figure 4. **Overview of the proposed method.** We identify a universal register by analyzing the inputs of quantization-sensitive layers across blocks. During inference, the register is inserted into each block, and outlier tokens are removed from the most quantization-sensitive layer.

Precisely, given some test image \mathbf{x}_{test} , we select the tokens with the top- \tilde{k} ℓ_∞ norm, *i.e.*,

$$\mathcal{D} = \text{argtopk}\{\|\mathbf{z}\|_\infty \mid \mathbf{z} \in \Phi_{l_q}(\mathbf{x}_{\text{test}})\} \quad (2)$$

and remove these tokens from the model. Here, similarly to the curating and caching steps, the number of tokens to be removed—*i.e.*, \tilde{k} —is tuned using the reference task.

5. Experiments

In this section, we first describe the experimental setup in Sec. 5.1. We then present zero-shot image classification and image–text retrieval results in Sec. 5.2, showing that combining RegCache with either naïve quantization or other baseline algorithms yields a significant performance gain. Furthermore, we validate our design choices through ablation studies, analyze the behavior of prefix tokens, and assess the generalizability of the pre-computed prefix tokens.

5.1. Setup

Vision encoders. We evaluate the proposed method on five widely used vision encoders: (1) CLIP [29], (2) OpenCLIP [5], (3) SigLIP [43], (4) SigLIP2 [34], and (5) DINOv2 [27]. These vision encoders, widely used in various downstream tasks, cover diverse training configuration. Specifically, CLIP and SigLIP are trained on image–text pairs with contrastive objectives, whereas DINOv2 is trained on image-only datasets. Regarding input tokens, CLIP and DINOv2 utilize a class token to extract global features, while SigLIP and SigLIP2 use patch-wise pooling to generate a token that captures global information.

Evaluation. We evaluate the quality of the quantized vision encoders by measuring the zero-shot accuracy on two downstream tasks: (1) image classification on ImageNet-1k [8] and (2) text-image retrieval on MS-COCO [21]. To further validate the generalizability of the prefix searched from ImageNet-1k, evaluation is conducted on a diverse

set of image classification benchmarks, including Stanford Cars [18], Flowers-102 [26], Food-101 [3], and CIFAR-100.

Base quantization algorithms and details. To assess the broad applicability of RegCache as an effective on-top method, we define three classes of baseline strategies for activation quantization for ViTs: (1) architecture-specific quantizer designs that mitigate activation-distribution bottlenecks, (2) input-side distribution shaping to reduce quantization error. Specifically, we use PTQ4ViT [42] and RepQ-ViT [19] for (1) and NoisyQuant [22] for (2). Further details can be found in Sec. C.

Each baseline adopts per-tensor dynamic quantization with 8-bit, 6-bit, and 4-bit integer precision, using 1,024 and 32 calibration samples and for NoisyQuant and RepQ-ViT, respectively, as in original papers. Additionally, for CLIP and SigLIP models, prefixes are inserted from the searched layer to the final layer. DINOv2, trained in a self-supervised manner, exhibits different behavior compared to CLIP and SigLIP models; consequently, we find that inserting the prefix only at the searched layer yields better results.

5.2. Experimental results

Main results. In Tab. 2, we report the zero-shot image classification accuracy on ImageNet-1k dataset. We observe that the baselines combined with the RegCache consistently achieves better accuracy in most settings. Specifically, baselines with RegCache outperform the base quantization methods in terms of both best accuracy gap (Best Δ) and average accuracy gap (Average Δ). Only one setup—DINOv2-B—exhibits a negligible accuracy drop.

For zero-shot image–text retrieval (Tab. 3), we similarly observe that combining RegCache with the base quantization methods yields higher performance across all setups on average. These results indicate that RegCache can integrate well with other quantization methods across diverse tasks.

In particular, our method provides greater benefits when applied to low-precision quantization settings (*i.e.*, 4-bit and

Table 2. **Zero-shot classification accuracy of various vision encoders on ImageNet-1k.** We have used various base quantization algorithms to quantize to 4/6/8 bits. The best results are marked in **bold**. Best/Average Δ denote the gaps between the best/average performance of each baseline with and without RegCache, excluding the Naïve cases.

Method	CLIP-B/16			OpenCLIP-B/16			SigLIP-B/16			SigLIP2-B/16			DINOv2-B/14		
	W4A4	W6A6	W8A8	W4A4	W6A6	W8A8	W4A4	W6A6	W8A8	W4A4	W6A6	W8A8	W4A4	W6A6	W8A8
FP32	68.32			70.22			76.05			78.47			83.26		
Naïve	0.09	0.17	34.01	0.10	0.47	46.12	0.13	0.77	69.71	0.14	0.19	26.04	0.00	0.01	19.20
w/ RegCache	0.07	0.44	59.71	0.10	1.20	66.90	0.10	24.41	74.38	0.11	0.26	72.35	0.18	0.42	22.26
PTQ4ViT	0.37	51.60	67.69	0.09	59.98	69.39	0.19	68.68	75.57	0.28	41.54	76.92	0.01	78.28	82.97
w/ RegCache	1.78	55.30	67.86	0.14	63.58	69.61	0.59	72.38	75.75	2.67	68.17	76.88	2.38	78.55	82.92
RepQ-ViT	1.83	53.25	67.39	1.18	46.51	68.70	21.36	73.32	75.23	0.40	64.91	76.43	4.52	19.53	82.27
w/ RegCache	21.50	66.73	68.08	11.10	68.35	70.06	33.76	74.52	75.94	10.15	75.44	77.13	4.97	22.38	81.55
NoisyQuant	0.34	46.19	63.20	2.50	59.05	67.08	1.78	71.10	75.50	0.46	44.50	70.83	0.77	49.25	71.46
w/ RegCache	1.42	57.41	65.82	10.41	67.51	69.36	9.19	72.28	75.64	0.54	62.60	76.44	1.94	48.65	70.38
Best Δ	+19.67	+13.48	+2.62	+9.92	+21.84	+2.28	+12.40	+3.70	+0.71	+9.75	+26.63	+5.61	+2.37	+2.85	-0.05
Average Δ	+7.39	+9.47	+1.16	+5.86	+11.3	+1.29	+6.74	+2.03	+0.34	+4.07	+18.42	+2.09	+1.33	+0.84	-0.62

Table 3. **Zero-shot image–text retrieval performance of CLIP and SigLIP on MS-COCO under W6A6 and W8A8.** The best results are in **bold**. Best/Average Δ denote the gap between the best/average performances with and without RegCache for each baseline.

	(a) CLIP-B/16								(b) SigLIP-B/16							
	I \rightarrow T				T \rightarrow I				I \rightarrow T				T \rightarrow I			
	W6A6		W8A8		W6A6		W8A8		W6A6		W8A8		W6A6		W8A8	
	R@1	R@5	R@1	R@5	R@1	R@5	R@1	R@5	R@1	R@5	R@1	R@5	R@1	R@5	R@1	R@5
FP32	52.94	77.78	52.94	77.78	32.73	57.50	32.73	57.50	67.68	86.94	67.68	86.94	47.19	72.46	47.19	72.46
Naïve	0.00	0.12	22.76	41.92	0.06	0.28	14.08	30.43	0.34	1.12	60.04	82.66	0.86	2.67	41.80	67.40
w/ RegCache	0.22	0.74	46.10	71.68	0.44	1.28	28.02	52.03	12.06	25.22	65.76	86.00	12.70	27.16	46.30	71.23
PTQ4ViT	37.28	62.42	52.78	77.94	23.00	46.12	32.00	56.65	60.66	81.84	66.86	87.02	41.73	67.03	47.16	71.94
w/ RegCache	43.46	69.60	53.54	77.52	26.51	49.98	32.48	57.27	61.42	82.48	67.72	86.88	43.05	68.54	47.61	72.70
RepQ-ViT	29.06	53.48	44.52	68.64	15.90	35.22	23.01	45.20	37.50	60.46	65.90	86.78	26.42	48.73	46.33	71.48
w/ RegCache	38.68	63.90	45.58	69.64	19.70	40.91	23.68	46.44	61.06	83.32	66.12	86.78	43.63	68.83	46.42	71.48
NoisyQuant	25.26	47.66	48.94	74.10	18.02	39.08	31.07	56.18	52.52	77.42	67.10	86.96	33.36	58.30	46.76	72.05
w/ RegCache	33.86	57.84	49.10	73.20	22.28	44.27	30.40	55.20	63.28	83.96	67.24	86.92	43.25	68.83	47.64	72.62
Best Δ	+9.62	+10.42	+1.06	+1.00	+4.26	+5.69	+0.67	+1.24	+23.56	+22.86	+0.86	+0.00	+17.21	+20.10	+0.88	+0.76
Average Δ	+8.13	+9.26	+0.66	-0.11	+3.86	+4.91	+0.16	+0.29	+11.69	+10.01	+0.41	-0.06	+9.47	+10.71	+0.47	+0.44

6-bit), because the impact of activation outliers on quantization becomes correspondingly more severe; Low-bit results are also reported in Tab. 2 and Tab. 3.

Reducing token norm outliers. Tab. 5 illustrates the change in the maximum token norm of the quantization-sensitive layer input when RegCache is applied. As expected, the maximum token norm decreases. This reduction effectively narrows the dynamic range of quantization, thereby improving quantization performance.

Universality of prefixes. Since the prefix search procedure in RegCache involves validation on the training split of the ImageNet-1k dataset, we additionally assess whether the learned prefixes generalize to other datasets, as the register token might have overfit to ImageNet-1k. In this spirit, we perform zero-shot classification on other datasets, with

the results reported in Tab. 4. These results indicate that the prefix learned on ImageNet-1k remains effective on other datasets, suggesting that it acts as a universal register token.

Ablation study. To verify the design choice our method, we ablate the effect of our two stage methods—(1) prefix caching and (2) token deleting—by examining quantization performance. In Tab. 6, we present the ablation study results for SigLIP and SigLIP2. The results show that the two stages, prefix caching and token deleting, act synergistically, yielding the best performance when both components are used together for both vision encoders. Surprisingly, when only one of the two steps is applied, we obtain even worse results than in the naïve case, further supporting the validity of our design choice.

Other experiments. Beyond the main experiments, we

Table 4. **Zero-shot classification accuracy (%) on other image classification datasets.** The prefixes used in our method are searched using the training split of ImageNet-1K, to validate the generalizability of the proposed method.

Model	Method	StanfordCars	Flowers-102	Food-101	CIFAR-100
CLIP-B/16	FP32	64.41	65.88	85.22	68.44
	Naïve	29.76	26.20	33.30	35.96
	w/ RegCache	49.96 (+20.20)	55.39 (+29.19)	74.68 (+41.38)	51.87 (+15.91)
OpenCLIP-B/16	FP32	88.07	69.88	83.77	76.82
	Naïve	74.85	42.97	36.44	40.61
	w/ RegCache	85.85 (+11.00)	68.06 (+25.09)	80.80 (+44.36)	71.73 (+31.12)
SigLIP-B/16	FP32	90.81	82.63	89.34	72.33
	Naïve	87.97	75.26	78.31	54.79
	w/ RegCache	89.73 (+1.76)	80.32 (+5.06)	88.17 (+9.86)	66.87 (+12.08)
SigLIP2-B/16	FP32	92.74	83.38	90.65	77.10
	Naïve	35.12	26.38	30.55	20.92
	w/ RegCache	88.20 (+53.08)	76.50 (+50.12)	86.47 (+55.92)	59.78 (+38.86)

Table 5. **Reduction in maximum token norm within the input of quantization-sensitive layers in W8A8.** We report the mean across 500 image samples.

Model	Max token	
	Vanilla	w/ RegCache
CLIP	41.38	11.45
OpenCLIP	92.78	9.64
SigLIP	35.82	3.64
SigLIP2	148.20	15.16

conduct several additional experiments in the appendix. More concretely, we provide the following results:

- Combining with a recently proposed ViT quantization method, namely FIMA-Q [35] ▷ Sec. D
- Retrieval with other vision encoders ▷ Sec. F
- Combining with weight-only quantization ▷ Sec. G
- Computational efficiency analysis of RegCache, in terms of FLOPs and wall-clock time ▷ Sec. H
- Visualization of searched register tokens ▷ Sec. I
- Combining with outlier mitigation algorithms that use Hadamard rotation ▷ Sec. K

6. Conclusion

In this paper, we introduce a training-free outlier mitigation algorithm, *RegCache*. RegCache can serve as an on-top method, and it can be combined with existing PTQ algorithms for large-scale transformer-based vision encoders. Through extensive experiments, we demonstrate that RegCache consistently improves quantization performance across various tasks, indicating that it is indeed synergistic with other quantization methods. Our analyses reveal that RegCache effectively suppresses the activation

Table 6. **Ablation studies.** We compare the contribution of each component of RegCache on SigLIP-B/16 and SigLIP2-B/16. Caching and deleting plays a complementary role, enabling a wide coverage over a wide range of vision encoders.

Method	SigLIP-B/16	SigLIP2-B/16
Baseline	69.71	26.04
Prefix Caching	74.37	23.82
Token Deleting	42.41	69.06
Prefix Caching + Token Deleting	74.38	72.35

outliers in quantization-sensitive layers, thereby narrowing the dynamic range of the input and improving quantization performance. Furthermore, we take a step toward identifying register tokens that are optimal for the quantization of vision encoders—a task that is inherently more elusive than for language models.

Limitations. A major limitation of our method is the need to tune several additional hyperparameters, such as the maximum number of tokens to delete and the number of prefix tokens. Another limitation is that the number of prefix and deleted tokens must be selected heuristically for each vision encoder and base quantization algorithm.

Discussions and future directions. Our work covers a variety of vision encoders, including those trained on multimodal data (e.g., CLIP) and those trained on vision-only data (e.g., DINOv2). In our experiments, we observe that quantization-related measures (e.g., quantization sensitivity) behave somewhat differently across these cases, warranting further study. Another research direction arises from the differences between LLMs and ViT-based vision encoders: their outlier behavior differs significantly (see Sec. J for an extended discussion). Understanding this phe-

nomenon would benefit wide range of domains, including quantization and representation learning.

7. acknowledgment

This work was supported in part by AI Research Hub Project (No.RS-2024-00457882) and in part by Institute of Information & communications Technology Planning & Evaluation (IITP) grant funded by the Korea government (MSIT) (No.RS-2019-II191906, Artificial Intelligence Graduate School Program (POSTECH)).

References

- [1] Saleh Ashkboos, Amirkeivan Mohtashami, Maximilian L Croci, Bo Li, Pashmina Cameron, Martin Jaggi, Dan Alisistar, Torsten Hoefer, and James Hensman. Quarot: Outlier-free 4-bit inference in rotated llms. *Advances in Neural Information Processing Systems*, 2024. 18
- [2] Yelysei Bondarenko, Markus Nagel, and Tijmen Blankevoort. Understanding and overcoming the challenges of efficient transformer quantization. In *Empirical Methods in Natural Language Processing*, 2021. 2
- [3] Lukas Bossard, Matthieu Guillaumin, and Luc Van Gool. Food-101-mining discriminative components with random forests. In *European conference on computer vision*, 2014. 6
- [4] Mengzhao Chen, Yi Liu, Jiahao Wang, Yi Bin, Wenqi Shao, and Ping Luo. Prefixquant: Eliminating outliers by pre-fixed tokens for large language models quantization. *arXiv preprint arXiv:2410.05265*, 2024. 1
- [5] Mehdi Cherti, Romain Beaumont, Ross Wightman, Mitchell Wortsman, Gabriel Ilharco, Cade Gordon, Christoph Schuhmann, Ludwig Schmidt, and Jenia Jitsev. Reproducible scaling laws for contrastive language-image learning. In *Proceedings of the IEEE/CVF conference on computer vision and pattern recognition*, 2023. 6
- [6] Yoni Choukroun, Eli Kravchik, Fan Yang, and Pavel Kisilev. Low-bit quantization of neural networks for efficient inference. In *IEEE/CVF International Conference on Computer Vision Workshop*, 2019. 1
- [7] Timothée Darct, Maxime Oquab, Julien Mairal, and Piotr Bojanowski. Vision transformers need registers. In *International Conference on Learning Representations*, 2024. 2, 3, 4, 16, 17
- [8] Jia Deng, Wei Dong, Richard Socher, Li-Jia Li, Kai Li, and Li Fei-Fei. Imagenet: A large-scale hierarchical image database. In *IEEE conference on computer vision and pattern recognition*, 2009. 6
- [9] Tim Dettmers, Mike Lewis, Younes Belkada, and Luke Zettlemoyer. GPT3.int8(): 8-bit matrix multiplication for transformers at scale. In *Advances in neural information processing systems*, 2022. 1, 2
- [10] Alexey Dosovitskiy, Lucas Beyer, Alexander Kolesnikov, Dirk Weissenborn, Xiaohua Zhai, Thomas Unterthiner, Mostafa Dehghani, Matthias Minderer, Georg Heigold, Sylvain Gelly, Jakob Uszkoreit, and Neil Houlsby. An image is worth 16x16 words: Transformers for image recognition at scale. In *International Conference on Learning Representations*, 2021. 1
- [11] Abhimanyu Dubey, Abhinav Jauhri, Abhishek Pandey, Abhishek Kadian, Ahmad Al-Dahle, Aiesha Letman, Akhil Mathur, Alan Schelten, Aobo Yang, Angela Fan, et al. The llama 3 herd of models. *arXiv preprint arXiv:2407.21783*, 2024. 17
- [12] Xiangming Gu, Tianyu Pang, Chao Du, Qian Liu, Fengzhuo Zhang, Cunxiao Du, Ye Wang, and Min Lin. When attention sink emerges in language models: An empirical view. In *International Conference on Learning Representations*, 2025. 17

- [13] Zhiyu Guo, Hidetaka Kamigaito, and Taro Watanabe. Attention score is not all you need for token importance indicator in kv cache reduction: Value also matters. In *Empirical Methods in Natural Language Processing*, 2024. 3
- [14] Nicholas Jiang, Amil Dravid, Alexei A Efros, and Yossi Gan- delsman. Vision transformers don't need trained registers. In *Advances in neural information processing systems*, 2025. 3, 4, 16, 19
- [15] Seil Kang, Jinyeong Kim, Junhyeok Kim, and Seong Jae Hwang. See what you are told: Visual attention sink in large multimodal models. In *International Conference on Learning Representations*, 2025. 3
- [16] Moo Jin Kim, Karl Pertsch, Siddharth Karamcheti, Ted Xiao, Ashwin Balakrishna, Suraj Nair, Rafael Rafailov, Ethan P Foster, Pannag R Sanketi, Quan Vuong, Thomas Kollar, Benjamin Burchfiel, Russ Tedrake, Dorsa Sadigh, Sergey Levine, Percy Liang, and Chelsea Finn. Openvla: An open-source vision-language-action model. In *Proceedings of The 8th Conference on Robot Learning*, 2025. 1
- [17] Olga Kovaleva, Saurabh Kulshreshtha, Anna Rogers, and Anna Rumshisky. BERT busters: Outlier dimensions that disrupt transformers. In *Findings of the ACL*, 2021. 2
- [18] Jonathan Krause, Michael Stark, Jia Deng, and Li Fei-Fei. 3d object representations for fine-grained categorization. In *Proceedings of the IEEE international conference on computer vision workshops*, 2013. 6
- [19] Zhikai Li, Junrui Xiao, Lianwei Yang, and Qingyi Gu. Repqvit: Scale reparameterization for post-training quantization of vision transformers. In *Proceedings of the IEEE/CVF International Conference on Computer Vision*, 2023. 3, 6, 13
- [20] Ji Lin, Jiaming Tang, Haotian Tang, Shang Yang, Wei-Ming Chen, Wei-Chen Wang, Guangxuan Xiao, Xingyu Dang, Chuang Gan, and Song Han. AWQ: Activation-aware weight quantization for on-device LLM compression and acceleration. In *Proceedings of Machine Learning and Systems*, 2024. 1, 15
- [21] Tsung-Yi Lin, Michael Maire, Serge Belongie, James Hays, Pietro Perona, Deva Ramanan, Piotr Dollár, and C Lawrence Zitnick. Microsoft coco: Common objects in context. In *European conference on computer vision*, 2014. 6
- [22] Yijiang Liu, Huanrui Yang, Zhen Dong, Kurt Keutzer, Li Du, and Shanghang Zhang. Noisyquant: Noisy bias-enhanced post-training activation quantization for vision transformers. In *Proceedings of the IEEE/CVF Conference on Computer Vision and Pattern Recognition*, 2023. 3, 6, 13
- [23] Zhenhua Liu, Yunhe Wang, Kai Han, Wei Zhang, Siwei Ma, and Wen Gao. Post-training quantization for vision transformer. *Advances in Neural Information Processing Systems*, 2021. 3
- [24] Zechun Liu, Changsheng Zhao, Igor Fedorov, Bilge Soran, Dhruv Choudhary, Raghuraman Krishnamoorthi, Vikas Chandra, Yuandong Tian, and Tijmen Blankevoort. Spinquant: LLM quantization with learned rotations. In *International Conference on Learning Representations*, 2025. 18
- [25] Andrew Lu, Wentinn Liao, Liuhui Wang, Huzheng Yang, and Jianbo Shi. Artifacts and attention sinks: Structured approximations for efficient vision transformers. *arXiv preprint arXiv:2507.16018*, 2025. 3
- [26] Maria-Elena Nilsback and Andrew Zisserman. Automated flower classification over a large number of classes. In *Indian conference on computer vision, graphics & image processing*, 2008. 6
- [27] Maxime Oquab, Timothée Darcet, Théo Moutakanni, Huy V. Vo, Marc Szafraniec, Vasil Khalidov, Pierre Fernandez, Daniel HAZIZA, Francisco Massa, Alaeldin El-Nouby, Mido Assran, Nicolas Ballas, Wojciech Galuba, Russell Howes, Po-Yao Huang, Shang-Wen Li, Ishan Misra, Michael Rabbat, Vasu Sharma, Gabriel Synnaeve, Hu Xu, Herve Jegou, Julien Mairal, Patrick Labatut, Armand Joulin, and Piotr Bojanowski. DINOv2: Learning robust visual features without supervision. *Transactions on Machine Learning Research*, 2024. 1, 6
- [28] Balamurugan Palanisamy, Vikas Hassija, Arpita Chatterjee, Arpita Mandal, Debanshi Chakraborty, Amit Pandey, G. S. S. Chalapathi, and Dhruv Kumar. Transformers for vision: A survey on innovative methods for computer vision. *IEEE Access*, 13:95496–95523, 2025. 1
- [29] Alec Radford, Jong Wook Kim, Chris Hallacy, Aditya Ramesh, Gabriel Goh, Sandhini Agarwal, Girish Sastry, Amanda Askell, Pamela Mishkin, Jack Clark, et al. Learning transferable visual models from natural language supervision. In *International conference on machine learning*, 2021. 1, 6
- [30] Oriane Siméoni, Huy V Vo, Maximilian Seitzer, Federico Baldassarre, Maxime Oquab, Cijo Jose, Vasil Khalidov, Marc Szafraniec, Seungeun Yi, Michaël Ramamonjisoa, et al. Dinov3. *arXiv preprint arXiv:2508.10104*, 2025. 2
- [31] Seungwoo Son, Wonpyo Park, Woohyun Han, Kyuyeun Kim, and Jaeho Lee. Prefixing attention sinks can mitigate activation outliers for large language model quantization. In *Empirical Methods in Natural Language Processing*, 2024. 1, 2, 3, 5
- [32] Mingjie Sun, Xinlei Chen, J Zico Kolter, and Zhuang Liu. Massive activations in large language models. In *Conference on Language Modeling*, 2024. 1, 2, 3, 17
- [33] William Timkey and Marten Van Schijndel. All bark and no bite: Rogue dimensions in transformer language models obscure representational quality. In *Empirical Methods in Natural Language Processing*, 2021. 2
- [34] Michael Tschannen, Alexey Gritsenko, Xiao Wang, Muhammad Ferjad Naeem, Ibrahim Alabdulmohsin, Nikhil Parthasarathy, Talfan Evans, Lucas Beyer, Ye Xia, Basil Mustafa, et al. Siglip 2: Multilingual vision-language encoders with improved semantic understanding, localization, and dense features. *arXiv preprint arXiv:2502.14786*, 2025. 6
- [35] Zhuguanyu Wu, Shihe Wang, Jiayi Zhang, Jiaxin Chen, and Yunhong Wang. Fima-q: Post-training quantization for vision transformers by fisher information matrix approximation. In *Proceedings of the Computer Vision and Pattern Recognition Conference*, 2025. 3, 8, 13
- [36] Zhuguanyu Wu, Jiayi Zhang, Jiaxin Chen, Jinyang Guo, Di Huang, and Yunhong Wang. Aphq-vit: Post-training quantization with average perturbation hessian based reconstruction for vision transformers. In *Proceedings of the Computer Vision and Pattern Recognition Conference*, 2025. 3

- [37] Guangxuan Xiao, Ji Lin, Mickael Seznec, Hao Wu, Julien Demouth, and Song Han. SmoothQuant: Accurate and efficient post-training quantization for large language models. In *International conference on Machine Learning*, 2023. 1
- [38] Guangxuan Xiao, Yuandong Tian, Beidi Chen, Song Han, and Mike Lewis. Efficient streaming language models with attention sinks. In *International Conference on Learning Representations*, 2024. 1, 3
- [39] Kai Yuanqing Xiao, Logan Engstrom, Andrew Ilyas, and Aleksander Madry. Noise or signal: The role of image backgrounds in object recognition. In *International Conference on Learning Representations*, 2021. 4
- [40] Jaewoo Yang, Hayun Kim, and Younghoon Kim. Mitigating quantization errors due to activation spikes in GLU-based LLMs. *arXiv preprint 2405.14428*, 2024. 1
- [41] Lianwei Yang, Haisong Gong, and Qingyi Gu. Dopqvit: Towards distribution-friendly and outlier-aware post-training quantization for vision transformers. *arXiv preprint arXiv:2408.03291*, 2024. 3
- [42] Zhihang Yuan, Chenhao Xue, Yiqi Chen, Qiang Wu, and Guangyu Sun. Ptq4vit: Post-training quantization for vision transformers with twin uniform quantization. In *European conference on computer vision*, 2022. 3, 6, 13
- [43] Xiaohua Zhai, Basil Mustafa, Alexander Kolesnikov, and Lucas Beyer. Sigmoid loss for language image pre-training. In *Proceedings of the IEEE/CVF international conference on computer vision*, 2023. 6
- [44] Tianchen Zhao, Tongcheng Fang, Haofeng Huang, Rui Wan, Widyadewi Soedarmadji, Enshu Liu, Shiyao Li, Zinan Lin, Guohao Dai, Shengen Yan, Huazhong Yang, Xuefei Ning, and Yu Wang. Vudit-q: Efficient and accurate quantization of diffusion transformers for image and video generation. In *International Conference on Learning Representations*, 2025.

Activation Quantization of Vision Encoders Needs Prefixing Registers

Appendix

A. Impact of activation outlier in quantization

To assess the impact of outliers on quantization, we control the quantization range at the token level. In Tab. 7, “w/ outliers” applies standard per-tensor quantization. In contrast, the “w/o outliers” setting excludes outlier tokens from the per-tensor range and quantizes them separately via per-token quantization. As a result, quantizing the outlier tokens separately shows a substantial performance improvement, which demonstrates that mitigating outliers is a critical problem in quantization.

Table 7. Comparison of quantization performance w/ and w/o outlier.

Model	Full Precision	w/ outlier	w/o outlier
CLIP-B/16	68.32	34.01	55.83 (+21.82)
OpenCLIP-B/16	70.22	46.12	65.43 (+19.31)
SigLIP-B/16	76.05	69.71	74.54 (+4.83)
SigLIP2-B/16	78.47	26.04	74.54 (+48.50)
DINOv2-B/16	83.26	19.20	76.58 (+57.38)

B. High cosine similarity of outlier tokens

In this section, we provide a simple explanation for why outlier tokens maintain high cosine similarity across images, as shown in Tab. 1.

As an stylized example, consider two distinct outlier tokens, each modeled as a “spiked” vector in which a single element has high magnitude. Lemma 1 says that the high cosine similarity over the outlier tokens can largely be attributed to two factors⁴: (i) the presence of a large-magnitude entries and (ii) the alignment of the corresponding entry indices (i.e., same or at least similar channels).

Lemma 1. Let $\mathbf{x}, \mathbf{y} \in \mathbb{R}^d$ and fix an index $i \in \{1, \dots, d\}$. Let $\mathbf{1}_i \in \mathbb{R}^d$ denote the one-hot vector whose i th entry is 1 and all other entries are 0. For $C \in \mathbb{R}^+$, define $\mathbf{x}' = \mathbf{x} + C\mathbf{1}_i$, $\mathbf{y}' = \mathbf{y} + C\mathbf{1}_i$. then the vectors asymptotically converge to each other, i.e.,

$$\lim_{C \rightarrow \infty} \frac{\langle \mathbf{x}', \mathbf{y}' \rangle}{\|\mathbf{x}'\|_2 \|\mathbf{y}'\|_2} = 1. \quad (3)$$

Moreover, for $\mathbf{y}'' = \mathbf{y} + C\mathbf{1}_j$, where $j \neq i$, then the vectors become asymptotically orthogonal to each other, i.e.,

$$\lim_{C \rightarrow \infty} \frac{\langle \mathbf{x}', \mathbf{y}'' \rangle}{\|\mathbf{x}'\|_2 \|\mathbf{y}''\|_2} = 0. \quad (4)$$

Proof. For the same-index case (Eq. (3)), we can write this explicitly as

$$\frac{\langle \mathbf{x}', \mathbf{y}' \rangle}{\|\mathbf{x}'\|_2 \|\mathbf{y}'\|_2} = \frac{\langle \mathbf{x}, \mathbf{y} \rangle + C(x_i + y_i) + C^2}{\sqrt{\|\mathbf{x}\|_2^2 + 2Cx_i + C^2} \sqrt{\|\mathbf{y}\|_2^2 + 2Cy_i + C^2}}, \quad (5)$$

where x_i (resp. y_i) denotes the i th entry of \mathbf{x} (resp. \mathbf{y}). Dividing numerator and denominator by C^2 , we get

$$\frac{1 + \frac{x_i + y_i}{C} + \frac{\langle \mathbf{x}, \mathbf{y} \rangle}{C^2}}{\sqrt{1 + \frac{2x_i}{C} + \frac{\|\mathbf{x}\|_2^2}{C^2}} \sqrt{1 + \frac{2y_i}{C} + \frac{\|\mathbf{y}\|_2^2}{C^2}}}. \quad (6)$$

As $C \rightarrow \infty$, all terms of order $1/C$ and $1/C^2$ vanish, and we get what we want. The case of the different-index (Eq. (4)) can be handled similarly. \square

Indeed, as shown in Fig. 1 (right), we find that across different images, outlier tokens tend to have similar magnitudes in certain coordinates (i.e., along specific channels shared across different tokens).

⁴There are some cases where each component has a small magnitude, yet the vectors are still similar to one another. In high dimensions, however, this rarely happens; for example, random vectors become almost orthogonal as the dimension tends to infinity. In vision encoders, the number of channels per token is typically large (e.g., 768 channels in CLIP and SigLIP families), which results in low similarity among non-outlier tokens (e.g., “Normal tokens” in Tab. 1).

C. Baselines and experimental settings

In this section, we briefly introduce baseline quantization methods and device setup for our experiments.

- **PTQ4ViT** [42] proposes a twin uniform quantizer to handle the unbalanced activation distributions found in ViTs, particularly after non-linearities such as Softmax and GELU.
- **RepQ-ViT** [19] addresses quantization bottlenecks by applying specialized preprocessing to sensitive layers, such as channel-wise quantization after LayerNorm and log2 quantization after Softmax.
- **NoisyQuant** [22] introduces a quantizer-agnostic strategy that adds fixed uniform bias to activations, thereby reducing the quantization error of heavy-tailed distributions.
- **FIMA-Q** [35] suggests to optimize the rounding function and scaling factor using effective Hessian-guided quantization loss.

The experiments are conducted using NVIDIA RTX 4090 GPU, supplemented by a mixture of RTX A6000 and A6000 Ada.

D. Additional results with recent quantization method

We apply our algorithm to FIMA-Q [35], a recent PTQ method for ViT models, and evaluate it at 4/6/8-bit precisions on two tasks: zero-shot image classification on ImageNet-1k and image–text retrieval on MS-COCO. As shown in Tab. 8 and Tab. 9, RegCache consistently improves FIMA-Q across all models. The performance gap becomes even more pronounced at lower bit precisions, demonstrating that RegCache is particularly effective in challenging, low-bit quantization regimes.

Table 8. Image classification accuracy under W4A4, W6A6, and W8A8.

Model / Method		W4A4	W6A6	W8A8
OpenCLIP-B/16	FP32		68.32	
	FIMA-Q	50.41	66.51	67.63
	w/ RegCache	62.08 (+11.67)	66.70 (+0.19)	67.86 (+0.23)
CLIP-B/16	FP32		70.22	
	FIMA-Q	60.09	67.24	68.53
	w/ RegCache	65.11 (+5.02)	68.62 (+1.38)	69.13 (+0.60)
SigLIP-B/16	FP32		76.05	
	FIMA-Q	76.05	76.06	76.06
	w/ RegCache	76.13 (+0.08)	76.12 (+0.06)	76.12 (+0.06)
SigLIP2-B/16	FP32		78.47	
	FIMA-Q	78.47	78.46	78.47
	w/ RegCache	78.38 (-0.09)	78.37 (-0.09)	78.37 (-0.10)

Table 9. Zero-shot retrieval on MS-COCO (I→T / T→I).

Model	Method	I → T						T → I					
		W4A4		W6A6		W8A8		W4A4		W6A6		W8A8	
		R@1	R@5										
CLIP-B/16	FP32	52.94	77.78	52.94	77.78	52.94	77.78	32.73	57.70	32.73	57.70	32.73	57.70
	FIMA-Q	40.92	68.58	52.90	77.70	53.58	77.80	27.71	52.04	32.33	57.24	32.76	57.64
	w/ RegCache	51.82	76.26	53.22	77.58	53.66	77.94	33.43	58.53	32.88	57.69	33.01	57.64
OpenCLIP-B/16	FP32	61.02	83.04	61.02	83.04	61.02	83.04	41.38	66.93	41.38	66.93	41.38	66.93
	FIMA-Q	55.82	79.50	58.84	81.56	59.26	82.22	38.02	64.01	40.39	66.14	40.21	66.08
	w/ RegCache	57.34	80.70	59.86	82.20	59.86	82.20	40.02	65.38	40.30	66.18	40.58	66.42
SigLIP-B/16	FP32	67.68	86.94	67.68	86.94	67.68	86.94	47.19	72.46	47.19	72.46	47.19	72.46
	FIMA-Q	67.66	86.98	67.70	86.98	67.62	86.96	47.23	72.47	47.22	72.44	47.21	72.45
	w/ RegCache	68.14	87.04	68.14	87.00	68.18	87.04	47.64	72.78	47.62	72.80	47.62	72.81
SigLIP2-B/16	FP32	71.60	89.16	71.60	89.16	71.60	89.16	52.33	76.58	52.33	76.58	52.33	76.58
	FIMA-Q	67.70	86.98	67.68	86.98	67.70	86.98	47.22	72.44	47.21	72.45	47.22	72.44
	w/ RegCache	71.54	89.24	71.54	89.24	71.52	89.20	52.49	76.66	52.49	76.66	52.50	76.64

E. Additional results of quantization sensitivity

In this section, we provide additional plots for other vision encoders, analogous to those in Figure 2. In Fig. 5, we plot layerwise quantization sensitivity (top row) and maximum token norm (bottom row) for OpenCLIP and SigLIP2. The trends are consistent with our analysis in Sec. 3.1: increases in maximum token norm coincide with decreases in quantization sensitivity. However, in the case of SigLIP2, the absolute scale of the maximum norm is significantly larger than in the other architectures we considered. Consequently, applying RegCache yields a clearer benefit, as shown in Tab. 2. Given SigLIP2’s distinct behavior compared to other vision encoders, it would be intriguing to investigate further; we leave this for future work.

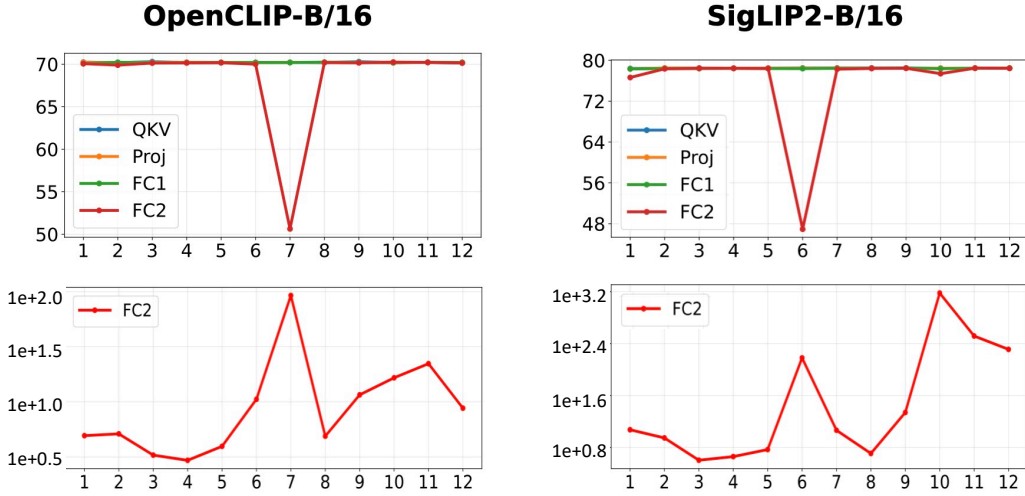


Figure 5. **(Top)** Layerwise quantization sensitivity (%). Zero-shot ImageNet-1k accuracy when we quantize only one layer to W8A8. **(Bottom)** Layerwise max token norms. The largest ℓ_∞ -norm of all tokens in an image on a logarithmic scale, averaged over the ImageNet-1k validation set.

F. Additional results on image retrieval results

We presents supplementary tables for additional vision encoders, in a format consistent with Tab. 3. For other models, Tab. 10 presents zero-shot image–text retrieval results on the MSCOCO dataset for OpenCLIP and SigLIP2. In both models, RegCache consistently achieves the highest retrieval accuracy as well.

Table 10. Zero-shot image–text retrieval performance of OpenCLIP and SigLIP2 on MS-COCO under W6A6 and W8A8. The best results are in **bold**. Best/Average Δ denote the gap between the best/average performances with and without RegCache for each baseline.

(a) OpenCLIP-B/16										(b) SigLIP2-B/16										
	I → T				T → I					I → T				T → I						
	W6A6		W8A8		W6A6		W8A8			W6A6		W8A8		W6A6		W8A8				
	R@1	R@5	R@1	R@5	R@1	R@5	R@1	R@5		R@1	R@5	R@1	R@5	R@1	R@5	R@1	R@5			
FP32	61.02	83.04	61.02	83.04	41.38	66.93	41.38	66.93		71.60	89.16	71.60	89.16	52.33	76.58	52.33	76.58			
Naïve	0.16	0.46	37.32	61.12	0.24	0.80	26.30	49.38		0.02	0.18	14.26	27.76	0.16	0.63	13.86	28.63			
w/ RegCache	0.32	1.40	57.60	81.12	0.77	2.32	38.45	64.17		0.08	0.30	64.02	84.66	0.22	0.68	46.80	72.47			
PTQ4ViT	50.60	76.20	59.60	82.16	34.56	60.60	40.66	66.40		29.88	52.94	69.74	88.72	27.33	50.82	51.62	75.87			
w/ RegCache	60.00	82.58	60.00	82.58	40.96	66.45	40.96	66.45		53.90	77.10	70.12	88.26	39.96	65.00	51.68	76.07			
RepQ-ViT	17.60	35.54	57.62	80.80	8.90	22.06	38.88	64.33		57.00	79.06	69.20	87.72	39.20	64.49	50.15	74.54			
w/ RegCache	32.96	56.64	59.44	81.90	14.90	33.73	39.82	65.51		58.78	80.78	69.76	87.76	41.26	66.14	50.15	74.66			
NoisyQuant	43.86	69.10	53.84	78.00	27.05	50.36	34.50	59.45		28.74	49.98	62.04	83.46	25.28	47.19	46.32	71.36			
w/ RegCache	51.58	76.32	56.06	79.84	31.73	55.90	35.53	60.69		50.66	75.26	70.24	88.60	39.25	64.43	51.41	76.04			
Best Δ	+15.36	+21.10	+2.22	+1.84	+6.40	+11.67	+1.03	+1.24		+24.02	+25.28	+8.20	+5.14	+13.97	+17.24	+5.09	+4.68			
Average Δ	+10.83	+11.57	+1.48	+1.12	+5.69	+7.69	+0.76	+0.82		+15.91	+17.05	+3.05	+1.57	+9.55	+11.02	+1.72	+1.67			

G. Weight-only quantization

We evaluate the performance of weight-only quantization to assess the compatibility of RegCache with weight-centric methods, which are commonly employed to reduce memory and deployment cost. Specifically, we adopt AWQ [20]—a popularly adopted weight-only quantization algorithm—as the base method, using a group size of 128 and varying bitwidths of 8, 6, 4, and 3. Across all configurations, RegCache consistently improves performance over vanilla AWQ, demonstrating its complementary benefit even in memory-constrained quantization settings.

Table 11. Zero-shot image classification accuracy (%) under weight-only quantization (AWQ).

Model	FP32	Method	Weight-only (AWQ) Bits			
			W3A16	W4A16	W6A16	W8A16
CLIP-B/16	68.32	AWQ	62.08	66.73	67.80	68.05
		+ RegCache	63.08 (+1.00)	67.06 (+0.33)	67.94 (+0.14)	68.14 (+0.09)
OpenCLIP-B/16	70.22	AWQ	63.60	68.57	69.64	69.50
		+ RegCache	63.79 (+0.19)	68.57 (+0.00)	69.66 (+0.02)	69.51 (+0.01)
SigLIP-B/16	76.05	AWQ	72.47	75.50	75.85	75.86
		+ RegCache	72.51 (+0.04)	75.51 (+0.01)	75.91 (+0.06)	75.93 (+0.07)
SigLIP2-B/16	78.48	AWQ	71.58	76.50	77.49	77.12
		+ RegCache	71.51 (-0.07)	76.56 (+0.06)	77.49 (+0.00)	77.12 (+0.00)

H. Computational efficiency of RegCache

In terms of computational efficiency, we quantitatively assess the computational overhead induced by the proposed RegCache method by measuring the FLOPs⁵ and wall-clock time⁶. As summarized in Tab. 12, the increase in FLOPs due to RegCache remains minimal—no more than 0.2% of the total computation. Furthermore, in terms of latency, SigLIP, SigLIP2, and DINOv2 exhibit only marginal slowdowns relative to vanilla W8A8. By contrast, CLIP and OpenCLIP show a larger increase of approximately 5%, primarily due to the additional prefixes, which increase memory loading despite negligible FLOPs (up to 0.2%) overhead. In practice, this cost is not critical, as it can be easily mitigated through hardware-level caching.

Table 12. **Comparison of GFLOPs and latency on W8A8.** The best configuration selected by our method in RegCache.

Model	GFLOPs			Latency (m/s)		
	Vanilla	RegCache	Δ (%)	Vanilla	RegCache	Δ (%)
CLIP-B/16	35.26	35.33	+0.20	1m 43.77s	1m 50.03s	+5.69
OpenCLIP-B/16	35.25	35.31	+0.17	1m 34.23s	1m 39.31s	+5.12
SigLIP-B/16	35.53	35.26	-0.76	1m 43.57s	1m 43.75s	+0.17
SigLIP2-B/16	35.53	35.47	-0.17	1m 44.20s	1m 47.31s	+2.89
DINOv2-B/16	46.46	46.47	+0.02	2m 51.39s	2m 53.04s	+0.95

I. Visualization of register tokens

In Fig. 6, we visualize the top 5 prefix tokens, ranked by their effectiveness for quantization, which is measured by W8A8 zero-shot classification accuracy on ImageNet-1k. The results are consistent with prior findings [7, 14], revealing that the searched register tokens are located in background regions. We find that the searched register tokens commonly correspond to low-frequency regions surrounded by semantically uninformative patches.

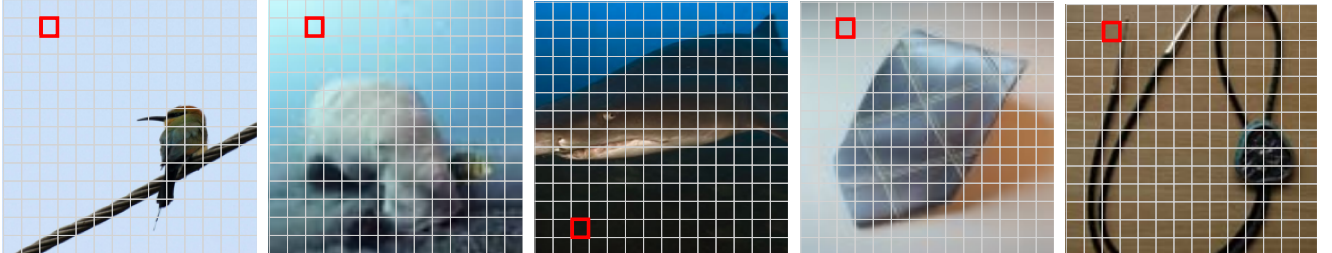


Figure 6. Visualization of register token searched from ImageNet-1k

⁵FLOPs are estimated per-image using a pseudo-quantization approach that simulates quantized operations.

⁶We measure wall-clock time as the inference time on the entire ImageNet-1k validation set.

J. Outliers in vision encoder vs. LLMs: A tokenization perspective

As shown in Fig. 2, various vision encoders exhibit outliers in the intermediate layers. Rewinding recent studies about outlier tendency in LLMs [12, 32], it is natural to ask: why do outliers consistently emerge in the intermediate layers of vision encoders, rather than in the early layers as in LLMs? In this section, we investigate this phenomenon by rethinking the difference of *tokenization strategies* between vision encoders and LLMs.

Roughly speaking, LLMs map input sequences to tokens drawn from a discrete, fixed vocabulary. In contrast, vision encoders and other ViT-based models process inputs by mapping them to continuous token embeddings using a (convolutional) neural network. We hypothesize that differences in the emergence of sink tokens can be attributed from their fundamentally distinct tokenization process.

To test this hypothesis, we compare the outlier behavior of DINOv2, pretrained both with and without learned register tokens, and LLaMA3-8B [11]. In this setup, the register tokens act as “fixed outlier sinks,” [7] effectively forming a closed-set vocabulary for outlier attraction, analogous to the tokenization setup in LLMs. As shown in Fig. 7, when ViTs are equipped with four learned register tokens, they begin to exhibit outliers in early layers (i.e., 2nd layer), mirroring the behavior observed in LLMs. This supports our hypothesis that continuous tokenization in ViTs plays a crucial role in the emergence of outliers in the intermediate layers.

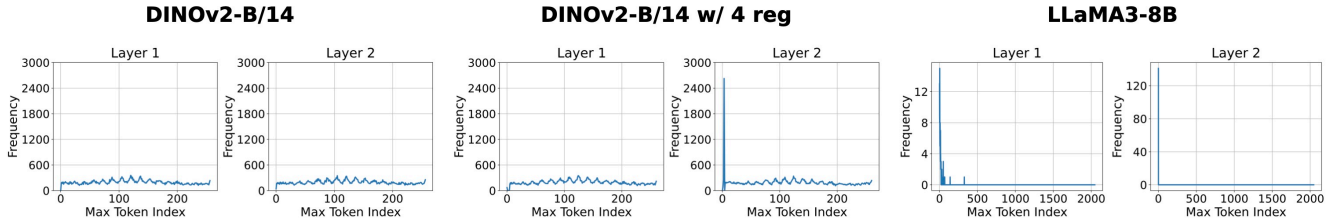


Figure 7. **The frequency of top-1 max tokens in the input tensor of FC2 layers in different models.** We evaluated DINOv2 on ImageNet-1K and LLaMA3-8B on Wikitext-2 dataset.

K. With Hadamard rotation quantization

Motivated by recent works in the LLM literature on utilizing Hadamard rotations for outlier mitigation [1, 24], we have also explored whether RegCache can also be combined with such methods. In particular, we follow the adaptations of ViDiT-Q [44] to apply Hadamard rotations to all linear layers in the transformer blocks.⁷ As reported in Tab. 13, RegCache improves accuracy when used as a plug-in method, indicating that suppressing extreme outliers in the rotated domain can further enhance quantization performance.

Table 13. Zero-shot image classification accuracy (%) on top of QuaRot [1]

Method	CLIP		OpenCLIP	
	W6A6	W8A8	W6A6	W8A8
FP32		68.32		70.22
Naïve	0.17	34.01	0.47	46.12
Quarot	55.86	66.38	59.49	68.50
Quarot + RegCache	56.05	66.84	59.76	68.50

L. Layerwise sensitivity to the prefix-insertion layer

In Fig. 8, we visualize how accuracy changes with the layer at which prefix insertion begins. As a result, accuracy drops sharply when insertion starts at layer 6—the layer right after the quantization-sensitive layer—indicating that prefix tokens are effective only when inserted before this sensitive layer. Based on this observation, we choose the intermediate layer as a initial prefix inserting layer to minimize a computational cost.

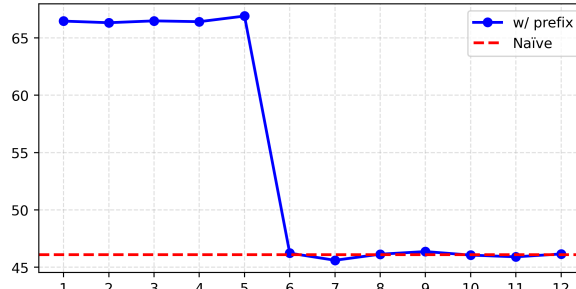


Figure 8. **Performance across prefix-insertion layers(%)**. The x-axis denotes the layer index where prefix insertion begins and the y-axis indicates zero-shot ImageNet-1k accuracy under W8A8 quantization.

⁷There is one exception: we do not use the Walsh–Hadamard matrix for the value and output projection matrices, as in the ViDiT-Q implementation. Also, we have empirically observed that naïvely applying QuaRot on vision encoders tend to severely damage the model performance.

Table 14. **Comparison with test-time register.** Accuracy of zero-shot image classification on ImageNet-1k under W8A8 quantization.

Method	CLIP-B/16	SigLIP-B/16
FP32	68.32	76.05
Naïve	34.01	69.71
Test-time register	44.30	73.81
RegCache	59.71	74.38

M. Comparison with test-time register

As mentioned in Sec. 2, Jiang et al. [14] propose register tokens to mitigate outlier in activation. In an extended experiment, they inject test-time registers as a form of KV cache while zeroing out outlier neurons, showing that high-norm outliers in the residual stream can be effectively suppressed.

To assess its practical effectiveness under quantization, we empirically evaluate this mechanism in a quantization setting and compare its performance directly against RegCache. As shown in Tab. 14, RegCache consistently outperforms the test-time register approach, indicating that it is more specifically optimized to mitigating outliers in quantized models.